AIP | Journal of Applied Physics

Temperature-dependent spin injection dynamics in InGaAs/GaAs quantum well-dot tunnel-coupled nanostructures

S. L. Chen, T. Kiba, X. J. Yang, J. Takayama, and A. Murayama

Citation: Journal of Applied Physics **119**, 115701 (2016); doi: 10.1063/1.4944039
View online: http://dx.doi.org/10.1063/1.4944039
View Table of Contents: http://scitation.aip.org/content/aip/journal/jap/119/11?ver=pdfcov
Published by the AIP Publishing

JOURNAL OF APPLIED PHYSICS **119**, 115701 (2016)

Temperature-dependent spin injection dynamics in InGaAs/GaAs quantum well-dot tunnel-coupled nanostructures

S. L. Chen,[1,a)] T. Kiba,[2] X. J. Yang,[3] J. Takayama,[1] and A. Murayama[1]
[1]*Graduate School of Information Science and Technology, Hokkaido University, Kita 14, Nishi 9, Kita-ku, Sapporo 060-0814, Japan*
[2]*Kitami Institute of Technology, 165 Koen-cho, Kitami, Hokkaido 090-8507, Japan*
[3]*Suzhou QiangMing Optoelectronics, Co. Ltd., Jiangsu, China*

(Received 22 November 2015; accepted 3 March 2016; published online 15 March 2016)

Time-resolved optical spin orientation spectroscopy was employed to investigate the temperature-dependent electron spin injection in $In_{0.1}Ga_{0.9}As$ quantum well (QW) and $In_{0.5}Ga_{0.5}As$ quantum dots (QDs) tunnel-coupled nanostructures with 4, 6, and 8 nm-thick GaAs barriers. The fast picosecond-ranged spin injection from QW to QD excited states (ES) was observed to speed up with temperature, as induced by pronounced longitudinal-optical (LO)-phonon-involved multiple scattering process, which contributes to a thermally stable and almost fully spin-conserving injection within 5–180 K. The LO-phonon coupling was also found to cause accelerated electron spin relaxation of QD ES at elevated temperature, mainly via hyperfine interaction with random nuclear field. © *2016 AIP Publishing LLC*. [http://dx.doi.org/10.1063/1.4944039]

I. INTRODUCTION

The nanosized "artificial atom" quantum dots (QDs) have been drawing enduring research interest since its appearance, owing to the fact their discrete electronic states created by three dimensional quantum confinement give rise to spectrally sharp radiative transitions with large oscillator strength and high optical yield. At the same time, spin relaxation process mediated by spin-orbit interaction via D'yakonov-Perel and Elliot-Yafet effect[1] is largely suppressed, leading to a prolonged spin lifetime at low temperature. Therefore, QDs are well-suited nanostructures for harnessing both photonic and spintronic functionalities, with promising application as spin-light-emitting/laser diodes (spin-LEDs/LDs) and spin qubits for quantum information technology.[2–4] An effective input of spins to QDs is crucial for spin-based device operation. Numerous studies have demonstrated quantum tunneling of charge carriers from quantum well (QW) to QDs as an efficient and controllable means for injection.[5–11] By further exploiting the spin degree of freedom, fast spin tunnel-injection based on InGaAs/GaAs QW-QD coupled structures has been achieved at 20 K,[12] which presents as a promising spin injector. However, knowledge about their performance at higher temperature, though important, remains unexplored. This is complicated by a multiple of thermally activated processes like carrier depopulation, accelerated spin-flips in both QW and QDs, enhanced carrier-phonon scattering rate, and so on. To clarify these issues which are essential for developing the room temperature-functioning spin injector, we present here a temperature-dependent study of electron spin injection dynamics in InGaAs/GaAs QW-QD tunnel-coupled nanostructures by using time-resolved optical spin orientation spectroscopy.

II. SAMPLES AND METHODS

The investigated samples were grown by molecular beam epitaxy (MBE). The QW has Indium alloy content [In] of 10%, with a thickness of 20 nm. While the lens-shaped QDs containing [In] of 50% are 20 nm (5 nm) in average basal diameter (height). Scanning electron microscopy (SEM) reveals a QD areal density, n_{QD}, of $\sim 2 \times 10^{10}\,cm^{-2}$. A set of three samples with different GaAs barrier thicknesses were prepared, i.e., $d_{Barrier} = 4$, 6, and 8 nm. In addition, a single QW with identical growth condition was used for reference. All samples show slightly p-type doping due to residual carbon acceptors in GaAs layer. The detailed information about growth can also be found in Ref. 12.

To perform the time-resolved optical spin orientation measurement, a mode-locked Ti: Sapphire pulsed laser with a repetition rate of 76 MHz and a temporal width of 150 fs was used, along with linear polarizer and quarter-wave plate, as circular-polarized excitation source. The laser output energy was tuned to 1.46 eV below GaAs barrier for resonant generation of spin-polarized carriers in QW, which are connected with QDs via wavefunction tunneling. The excitation power density is set to 5 W/cm^2. To avoid the Auger type of carrier scattering, we varied the pump fluence between 1.5 W/cm^2 and 15 W/cm^2 and found almost no change in rising of QD photoluminescence (PL) transients. Therefore, the spin-tunneled carriers energetically relax to localized QD excited states (ES) by predominant phonon emission. It should be noted a strong mixing of heavy and light hole subvalence bands in both well and dot can easily depolarize the hole spin orientation,[1,13–15] leaving electrons the major spin species in our study. The time-resolved PL from both QW and QDs of coupled structures was collected into a single grating monochromator and recorded by streak camera system with a temporal resolution of 5 ps. To differentiate the PL helicity, another set of linear polarizer and quarter-wave plate was used on detection side. By monitoring PL

a)Electronic mail: shuch@ist.hokudai.ac.jp

transients and circular polarization degree (*CPD*), defined as $CPD = (I_{\sigma+} - I_{\sigma-})/(I_{\sigma+} + I_{\sigma-})$, where $I_{\sigma+}$ ($I_{\sigma-}$) denotes the intensity of σ^+ (σ^-)-polarized PL component at QW ground state (GS) and QD ES, information on electron spin injection dynamics can be obtained.

III. RESULTS AND DISCUSSION

Figures 1(a)–1(c) show the PL spectra from all coupled structures at 5 K, which are strongly co-polarized with σ^+ laser excitation. The broad PL bands within 1.30 eV–1.38 eV stem from ES of ensemble QDs. Toward lower energy side, the PL intensity reduces drastically due to responsivity limit of our streak camera system, which results in a much weaker QD GS PL detection. To confirm, we measured the QD emission from a SpectrumOne CCD detector and clearly resolve a GS PL peak centered at 1.280 eV with a Full-Width-at-Half-Maximum (FWHM) of 60 meV after spectral deconvolution, see dashed line in Figure 1(a). Two ES labeled as "ES1" (1.331 eV) and "ES2" (1.383 eV) lie at higher energy side according to our computations of the electronic states based on Ref. 16, with an inter-level energy separation of ~50 meV. At 1.413 eV appears PL emission from QW GS, whose PL intensity increases with barrier thickness, reflecting the gradually decoupled wavefunction from QDs and hence stronger radiative recombination inside QW. The QW-QD wetting layer (WL) coupled state is observed, above QW GS, at 1.435 eV (not shown here). Due to its higher energy level and much thinner laser absorption region, the carriers are mainly photo-excited in the well and relax finally down to QW GS. Thus, the effect of WL in our PL measurement is negligibly small. The *CPD* calculated from circular-polarized PL of all samples is given as green line in Figures 1(a)–1(c). Due to laser excitation of both heavy and light hole exciton states in the well, which generates spin-down/up electrons in 3:1 ratio according to optical selection rule.[1,17] A "plateau-like" *CPD* value up to ~50% is observed at QW GS and higher-lying QD ES2 within 1.38 eV –1.42 eV. Toward lower detection energy, the *CPD* progressively decreases as a result of spin-dependent energy relaxation,[18,19] i.e., the spin blockade effect, and becomes close to zero at GS, indicating almost complete occupation of spin sub-levels. By raising temperature to, e.g., 105 K as shown in Figures 1(d)–1(f), the broad PL band of QDs blue-shifts due to thermal depopulation of carriers to higher-lying states, contributing to a progressively stronger PL from QW. Further increase in temperature significantly reduces emission from QD states and almost quenches it thermally about 180 K, as revealed by the spectrally integrated PL intensity ratio between QD and QW versus temperature in Figure 2. At the same time, the *CPD* across the entire spectral range decreases steadily, see Figures 1(d)–1(f), implying an enhanced spin relaxation process both in QDs and QW. In order to investigate the QW-to-QDs electron spin injection dynamics, we looked at the circular-polarized PL decays at QW GS and QD ES2, spectrally integrated over 1.40 eV–1.42 eV and 1.36 eV–1.38 eV, respectively. The resulting PL transients at 5 K are displayed in Figures 3(a)–3(c). As can be seen, both σ^+- and σ^--polarized PL traces of QW GS (open triangle) feature an intense fast decay. This initial PL transient is dominated by phonon-assisted carrier injection from QW to QD. Its time constant increases monotonously with barrier thickness as expected for reduced tunneling probability. At later time after initial injection follows a much slower PL trace, it reflects the recombination and spin relaxation dynamics of carriers quasi-equilibriumly distributed between QW and QD states. Looking at QD ES2, temporal evolution of *CPD* (solid star) was derived from circular-polarized time-resolved PL. By fitting with single-exponential function (dashed-dotted line), an electron spin relaxation time about 320 ps was derived for all samples, which is comparable to other reports.[18,20] With temperature increased to 105 K, see Figures 3(d)–3(f), phonon scattering process becomes increasingly important. This not only leads to an accelerated spin injection, i.e., faster initial decay as most clearly seen for 8 nm-barrier sample, but also a relatively stronger slow decay component due to thermalization of carriers from QD to QW via phonon

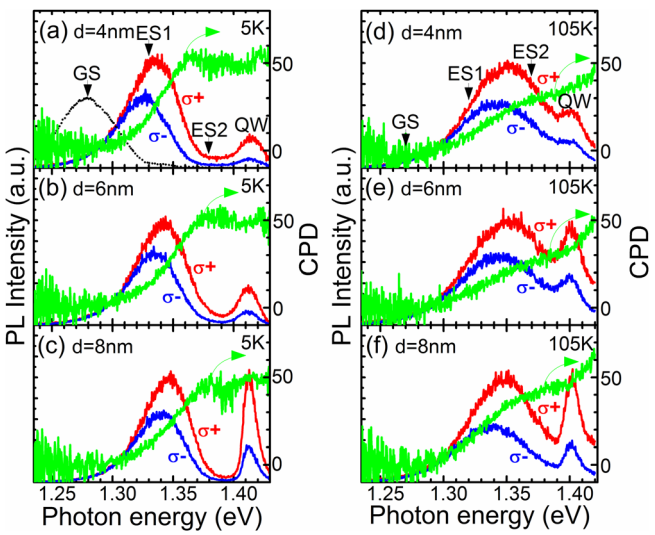

FIG. 1. 5 K (a)–(c) and 105 K (d)–(f) circular-polarized PL spectra and corresponding *CPD* from QW-QD tunnel-coupled structures with 4 nm, 6 nm, and 8 nm-thick barriers. The QD GS PL measured by another detector is shown as dashed line in (a).

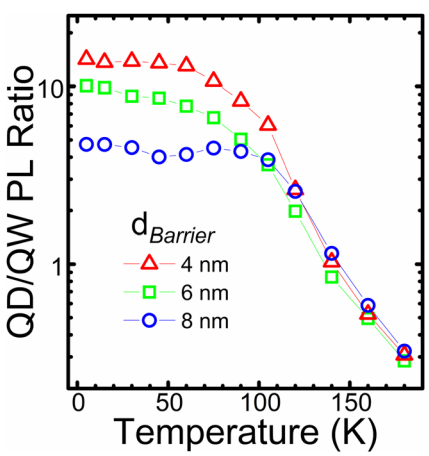

FIG. 2. PL intensity ratio between entire QD emission and QW as a function of temperature for samples with 4 nm, 6 nm, and 8 nm-thick barriers.

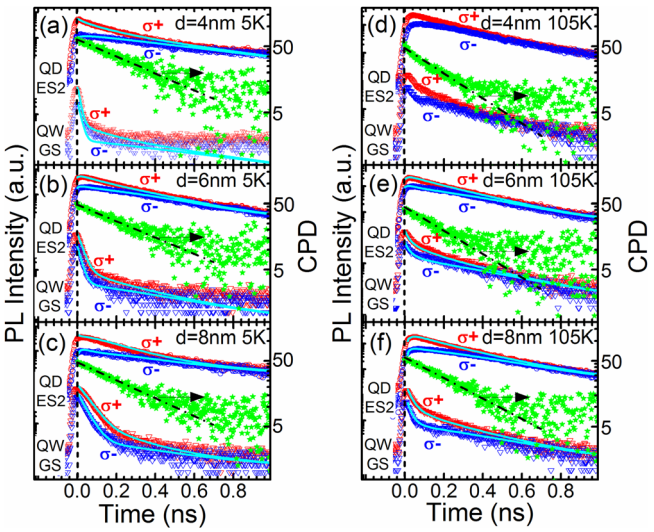

FIG. 3. Temperature-dependent circular-polarized PL decay from QW GS (open triangle) and QD ES2 (open dot) at 5 K (a)–(c) and 105 K (d)–(f). The time evolution of *CPD* for QD ES2 is displayed as solid stars and single-exponentially fitted by dashed-dotted line. Rate equation fittings to the experimental PL decays are shown as solid lines except for (d), due to limited time responsivity which is unable to resolve initial decay above 80 K (120 K) for 4 nm (6 nm)-thick barrier samples.

absorption. To quantitatively interpret the experimental PL decays and extract electron spin injection time, an effective three-level rate equation model was employed, which is illustrated in Figure 4 and written as

$$\frac{dN^{\pm}_{QW}}{dt} = -\frac{N^{\pm}_{QW}}{\tau^{rmb}_{QW}} - \frac{\left(N^{\pm}_{QW} - N^{\mp}_{QW}\right)}{2\tau^{s}_{QW}} - \frac{N^{\pm}_{QW}}{\tau_{inj}}\left(1 - \frac{N^{\pm}_{QD,ES2}}{D_{QD,ES2}}\right) + \frac{N^{\pm}_{QD,ES2}}{\tau_{inj}e^{\frac{\Delta E_2}{k_B T}}}, \quad (1)$$

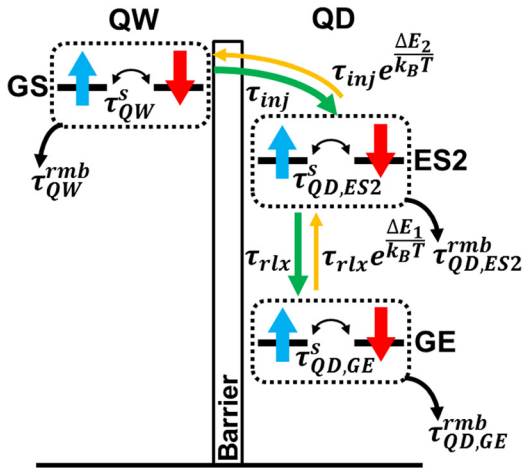

FIG. 4. Schematic diagram depicting electron spin injection and relaxation dynamics in QW-QD coupled structure. The QD GS and ES1 are summarized into an effective state labeled as GE. τ_i^{rmb} and τ_i^{s} (i: QW, QD ES2, and QD GE) denote recombination and electron spin relaxation time at each level. The spin injection (energy relaxation) to (in) QDs is characterized by τ_{inj} (τ_{rlx}), the thermalization process of which is associated with the factor $e^{\frac{\Delta E_{2(1)}}{k_B T}}$.

$$\frac{dN^{\pm}_{QD,ES2}}{dt} = -\frac{N^{\pm}_{QD,ES2}}{\tau^{rmb}_{QD,ES2}} - \frac{\left(N^{\pm}_{QD,ES2} - N^{\mp}_{QD,ES2}\right)}{2\tau^{s}_{QD,ES2}} + \frac{N^{\pm}_{QW}}{\tau_{inj}}\left(1 - \frac{N^{\pm}_{QD,ES2}}{D_{QD,ES2}}\right) - \frac{N^{\pm}_{QD,ES2}}{\tau_{inj}e^{\frac{\Delta E_2}{k_B T}}} - \frac{N^{\pm}_{QD,ES2}}{\tau_{rlx}}\left(1 - \frac{N^{\pm}_{QD,GE}}{D_{QD,GE}}\right) + \frac{N^{\pm}_{QD,GE}}{\tau_{rlx}e^{\frac{\Delta E_1}{k_B T}}}\left(1 - \frac{N^{\pm}_{QD,ES2}}{D_{QD,ES2}}\right), \quad (2)$$

$$\frac{dN^{\pm}_{QD,GE}}{dt} = -\frac{N^{\pm}_{QD,GE}}{\tau^{rmb}_{QD,GE}} - \frac{\left(N^{\pm}_{QD,GE} - N^{\mp}_{QD,GE}\right)}{2\tau^{s}_{QD,GE}} + \frac{N^{\pm}_{QD,ES2}}{\tau_{rlx}}\left(1 - \frac{N^{\pm}_{QD,GE}}{D_{QD,GE}}\right) - \frac{N^{\pm}_{QD,GE}}{\tau_{rlx}e^{\frac{\Delta E_1}{k_B T}}}\left(1 - \frac{N^{\pm}_{QD,ES2}}{D_{QD,ES2}}\right). \quad (3)$$

Here, $N_i^{\pm}$ (i: QW, QD ES2, and QD GE) denote spin population emitting $\sigma^{\pm}$-polarized PL at associated energy levels. The overall contribution from QD GS and ES1 is summarized as QD GE. The spin density of states is denoted as D_i, which is determined by single dot orbital degeneracy and QD density via $D_{QD,ES2\,(GE)} = 3 \times n_{QD}$. The rate equation accounts for three dynamical processes, (1) recombination, (2) spin-flip between degenerate spin sublevels, and (3) phonon-assisted energy relaxation (thermalization) to lower (upper) states, which are characterized by τ_i^{rmb}, τ_i^{s}, and $\tau_{inj/rlx}$ ($\tau_{inj/rlx}e^{\frac{\Delta E_{1,2}}{k_B T}}$), respectively. $\Delta E_{1(2)}$ is energy separation between QD ES2 and QD GE (QW GS and QD ES2). Though a multiple of time constants are introduced in the equations, most of them can be derived from PL measurement. To obtain τ^{rmb}_{QW} and τ^{s}_{QW} of QW, a reference single QW sample was measured, the results of which are displayed in Figure 5(b) as open and solid stars. The recombination time of QD ES2, $\tau^{rmb}_{QD,ES2}$, is derived from PL decay as 0.4 ns, its spin relaxation time, $\tau^{s}_{QD,ES2}$, is given in Figure 5(a) for different barrier thicknesses. $\tau^{rmb}_{QD,GE}$ of QD GE is measured to be 1.1 ns, and $\tau^{s}_{QD,GE}$ is 0.7 ns as determined from our previous work on the QD sample of same condition.[21] The temporal difference in PL rising of QD ES2 and GE defines a phonon relaxation time, τ_{rlx}, about 30 ps. Due to inhomogeneous broadening of each QD state, the effective energy separation, $\Delta E_{1(2)}$, and spin injection time, τ_{inj}, are set as fitting parameters. Best fittings to the experimental PL transients are shown as solid lines in Figure 3, yielding $\Delta E_{1(2)}$ of 30 meV (15 meV). The derived energy spacing is somehow smaller than that marked in Figure 1(a), which is most likely caused by QD size distribution, i.e., the smaller dots at higher energy side are easier to be thermalized to QW GS. The resulting spin injection time, τ_{inj}, is plotted in Figure 5(b). Due to limited time responsivity of streak camera, injection dynamics faster than 5 ps was unable to resolve. At 5 K, τ_{inj} amounts to 8 ps (4 nm), 12 ps (6 nm), and 24 ps (8 nm) for different barrier thicknesses. Thermally promoted

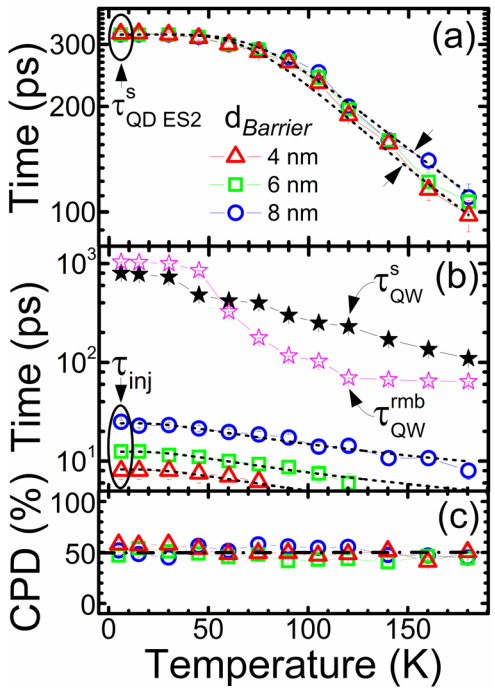

FIG. 5. The temperature dependence of electron spin relaxation time, $\tau^s_{QD,ES2}$, at QD ES2, phonon-assisted carrier injection time, τ_{rlx}, and initial *CPD*, $CPD_{t=0}$, of QD ES2 is summarized in (a), (b), and (c), respectively, for 4 nm (triangle), 6 nm (square), and 8 nm (dot) barrier samples. For comparison, a reference single QW sample was measured, whose recombination, τ^{rmb}_{QW}, and electron spin relaxation time, τ^s_{QW}, are displayed as open and solid stars in (b). Fittings to $\tau^s_{QD,ES2}$ and τ_{inj} are provided as dashed lines.

phonon scattering at higher temperature steadily accelerates the spin injection time, following a trend determined by phonon occupancy function,[22–24] i.e.,

$$\tau_{inj}^{-1} = \Gamma_0 \times [N_{ph}(T) + 1], \tag{4}$$

where Γ_0 is transition rate at 0 K, $N_{ph}(T)$ is Bose-Einstein distribution function, $N_{ph}(T) = [\exp(-E_{ph}/k_BT) - 1]^{-1}$. It should be noted that our measurement was performed on carrier injection from QW to an ensemble of inhomogeneously broadened QD ES. Therefore, E_{ph} measures the average phonon energy involved during the carrier injection. The temperature dependence of τ_{inj} can be well accounted by Equation (4) with $E_{ph} \approx 10$ meV for all samples. Since the phonon-assisted electron spin injection occurs at picosecond time range with transition rate up to $\sim 10^{12}$/s, which is much higher than the longitudinal-acoustical (LA) phonon scattering ($\sim 10^7$/s) with a threshold energy around 2.8 meV,[22,23] a multiple phonon scattering process involving dominant contribution from longitudinal-optical (LO) phonon is essential for energy dissipation. A speeding phonon relaxation with temperature is beneficial for fast spin injection, while another factor is also important in determining the spin injection efficiency, i.e., electron spin dynamics at QW GS. As can been seen in Figure 5(b), τ^s_{QW} gives a value of 800 ps at 5 K and decreases drastically with temperature, governed by D'yakonov-Perel effect.[1,17] However, it is still one order of magnitude longer than τ_{inj}, indicating that optically oriented electron spins can be efficiently transferred into QD before they are depolarized in QW. Indeed, QD ES2 for all coupled structures gives a temperature-stable initial *CPD* ($CPD_{t=0}$) of ~50%, as shown in Figure 5(c). By recalling a photo-excited 50% electron spin polarization in QW, this demonstrates an almost fully spin-conserving injection. The spin relaxation time, $\tau^s_{QD,ES2}$, of electron injected to QD ES2 remains ~320 ps at low temperature and drops drastically above 50 K, finally reaching ~100 ps at 180 K, see Figure 5(a). Phonon coupling is well known to account for increased electron spin depolarization at elevated temperature via phonon-assisted spin-orbit coupling[25–30] and electron-nuclear spin hyperfine interaction,[31–34] the latter of which is considered the main source of spin relaxation due to its stronger interaction strength.[31,34] Based on this, we adopted a reported model of two phonon scattering-mediated hyperfine interaction to account for the temperature dependence and estimate the phonon energy involved, which is expressed as[34]

$$\tau_s(T)^{-1} = \tau_s(0)^{-1} + \gamma N_{ph}(T)[N_{ph}(T) + 1], \tag{5}$$

where $\tau_s(0)$ is temperature-independent spin relaxation time, and the proportionality factor γ sums over all electron-phonon coupling matrix elements involved in scattering. Equation (5) was used to fit the upper and lower bound of $\tau^s_{QD,ES2}$ for all samples, shown as dashed line in Figure 5(a), and obtain a E_{ph} ranging within 28–30 meV. The derived phonon energy is comparable with that of LO phonon (32–33 meV),[24,35,36] thus pointing out its role in promoting the electron spin relaxation at elevated temperature.

IV. CONCLUSIONS

To summarize, we have studied temperature-dependent electron spin injection dynamics in InGaAs/GaAs QW-QD tunnel-coupled structures by optical spin orientation spectroscopy. Pronounced LO-phonon-involved scattering has been found to contribute to both fast and thermally stable electron spin injection from QW to QDs, rendering the tunnel-coupled structures an efficient spin injector for opto-spintronic devices. The LO-phonon coupling also accounts for the accelerated electron spin relaxation of QD ES at elevated temperature, mainly via hyperfine interaction with random nuclear spins in the QDs.

ACKNOWLEDGMENTS

The authors acknowledge the financial support of the Japan Society for the Promotion of Science (JSPS) via Grant-in-Aid for Scientific Research (S) No. 22221007 and the bilateral program promoted by JSPS.

[1]M. I. Dyakonov, *Spin Physics in Semiconductor* (Springer, Berlin Heidelberg, 2008).
[2]M. Holub and P. Bhattacharya, J. Phys. D: Appl. Phys. **40**, R179 (2007).
[3]D. D. Awschalom, D. Loss, and N. Samarth, *Semiconductor Spintronics and Quantum Computation* (Springer, 2002).
[4]D. Loss and D. P. DiVincenzo, Phys. Rev. A **57**, 120 (1998).
[5]Yu. I. Mazur, V. G. Dorogan, E. Marega, Jr., D. Guzun, M. E. Ware, Z. Ya. Zhuchenko, G. G. Tarasov, C. Lienau, and G. J. Salamo, J. Appl. Phys. **113**, 034309 (2013).
[6]C. Y. Jin, S. Ohta, M. Hopkinson, O. Kojima, T. Kita, and O. Wada, Appl. Phys. Lett. **96**, 151104 (2010).

[7]Yu. I. Mazur, V. G. Dorogan, E. Marega, Jr., Z. Ya. Zhuchenko, M. E. Ware, M. Benamara, G. G. Tarasov, P. Vasa, C. Lienau, and G. J. Salamo, J. Appl. Phys. **108**, 074316 (2010).
[8]D. Guzun, Yu. I. Mazur, V. G. Dorogan, M. E. Ware, E. Marega, Jr., G. G. Tarasov, C. Lienau, and G. J. Salamo, J. Appl. Phys. **113**, 154304 (2013).
[9]M. Syperek, J. Andrzejewski, W. Rudno-Rudzinski, G. Sek, J. Misiewicz, E. M. Pavelescu, C. Gilfert, and J. P. Reithmaier, Phys. Rev. B **85**, 125311 (2012).
[10]Yu. I. Mazur, V. G. Dorogan, D. Guzun, E. Marega, Jr., G. J. Salamo, G. G. Tarasov, A. O. Govorov, P. Vasa, and C. Lienau, Phys. Rev. B **82**, 155413 (2010).
[11]M. Syperek, P. Leszczynski, J. Misiewicz, E. M. Pavelescu, C. Gilfert, and J. P. Reithmaier, Appl. Phys. Lett. **96**, 011901 (2010).
[12]X. J. Yang, T. Kiba, T. Yamamura, J. Takayama, A. Subagyo, K. Sueoka, and A. Murayama, Appl. Phys. Lett. **104**, 012406 (2014).
[13]R. Ferreira and G. Bastard, Phys. Rev. B **43**, 9687 (1991).
[14]T. Uenoyama and L. J. Sham, Phys. Rev. Lett. **64**, 3070 (1990).
[15]T. Uenoyama and L. J. Sham, Phys. Rev. B **42**, 7114 (1990).
[16]A. Wojs, P. Hawrylak, S. Fafard, and L. Jacak, Phys. Rev. B **54**, 5604 (1996).
[17]F. Meier and B. P. Zakharchenya, *Optical Orientation* (North-Holland, Amsterdam, 1984).
[18]V. K. Kalevich, M. Paillard, K. V. Kavokin, X. Marie, A. R. Kovsh, T. Amand, A. E. Zhukov, Yu. G. Musikhin, V. M. Ustinov, E. Vanelle, and B. P. Zakharchenya, Phys. Rev. B **64**, 045309 (2001).
[19]T. Kiba, X. J. Yang, T. Yamamura, Y. Kuno, A. Subagyo, K. Sueoka, and A. Murayama, Appl. Phys. Lett. **103**, 082405 (2013).
[20]A. Tackeuchi, R. Ohtsubo, K. Yamaguchi, M. Murayama, T. Kitamura, T. Kuroda, and T. Takagahara, Appl. Phys. Lett. **84**, 3576 (2004).
[21]Y. Q. Huang, Y. Puttisong, I. A. Buyanova, X. J. Yang, A. Subagyo, K. Sueoka, A. Murayama, and W. M. Chen, Appl. Phys. Lett. **106**, 093109 (2015).
[22]T. Inoshita and H. Sakaki, Phys. Rev. B **46**, 7260 (1992).
[23]B. Ohnesorge, M. Albrecht, J. Oshinowo, and A. Forchel, Phys. Rev. B **54**, 11532 (1996).
[24]M. De Giogi, C. Lingk, G. von Plessen, J. Feldmann, S. De Rinaldis, A. Passaseo, M. De Vittorio, R. Cingolani, and M. Lomascolo, Appl. Phys. Lett. **79**, 3968 (2001).
[25]A. V. Khaetskii and Y. V. Nazarov, Phys. Rev. B **64**, 125316 (2001).
[26]S. I. Erlingsson, Y. V. Nazarov, and V. I. Fal'ko, Phys. Rev. B **64**, 195306 (2001).
[27]Y. G. Semenov and K. W. Kim, Phys. Rev. B **75**, 195342 (2007).
[28]R. Hanson, L. P. Kouwenhoven, J. R. Petta, S. Tarucha, and L. M. Vandersypen, Rev. Mod. Phys. **79**, 1217 (2007).
[29]E. Tsitsishvili, G. S. Lozano, and A. O. Gogolin, Phys. Rev. B **70**, 115316 (2004).
[30]D. V. Bulaev and D. Loss, Phys. Rev. B **71**, 205324 (2005).
[31]F. G. G. Hernandez, A. Greilich, F. Brito, M. Wiemann, D. R. Yakovlev, D. Reuter, A. D. Wieck, and M. Bayer, Phys. Rev. B **78**, 041303(R) (2008).
[32]B. Urbaszek, P. F. Braun, T. Amand, O. Krebs, T. Belhadj, A. Lemaitre, P. Voisin, and X. Marie, Phys. Rev. B **76**, 201301(R) (2007).
[33]J. Beyer, Y. Puttisong, I. A. Buyanova, S. Suraprapapich, C. W. Tu, and W. M. Chen, Appl. Phys. Lett. **100**, 143105 (2012).
[34]X. M. Dou, B. Q. Sun, D. S. Jiang, H. Q. Ni, and Z. C. Niu, J. Appl. Phys. **111**, 053524 (2012).
[35]A. Pinczuk, J. M. Worlock, R. E. Nahory, and M. A. Polack, Appl. Phys. Lett. **33**, 461 (1979).
[36]P. F. Lu, D. C. Tsui, and H. M. Cox, Phys. Rev. Lett. **54**, 1563 (1985).